THE ASTROPHYSICAL JOURNAL, 316:584–596, 1987 May 15

EXTENDED EMISSION-LINE REGIONS AROUND QSOs

ALAN STOCKTON[1]
Institute for Astronomy, University of Hawaii, and Royal Observatory, Edinburgh
AND
JOHN W. MACKENTY
Institute for Astronomy, University of Hawaii
Received 1986 August 13; accepted 1986 October 28

ABSTRACT

We describe a narrow-band [O III] λ5007 imaging survey of a sample of 47 luminous low-redshift QSOs. About 25% of the QSOs observed show luminous and highly structured emission-line regions, typically extending over a few tens of kpc. The distribution of the emission-line gas generally differs substantially from that of the stars. as inferred from line-free continuum images, indicating that we are not simply observing interstellar gas photoionized *in situ*.

From our spectrophotometry of all QSOs in the sample, we find a correlation between narrow-line luminosity in the nuclear region and the presence of strong extended emission; we also generally confirm the relation found by Boroson and Oke between radio spectral index and extended optical emission.

A substantial fraction of the QSOs with strong extended emission also have either close companion galaxies or apparent bridges or tails seen in continuum light, making it attractive to suppose that the gas is debris from tidal interactions or mergers. Whether or not this specific interpretation is correct, the fact that these emission regions seem to be both transient and quite common suggest that they are intimately connected with the physical mechanism responsible for the QSO activity itself.

Subject heading: quasars

I. INTRODUCTION

There is now good evidence that powerful nuclear activity in galaxies not only requires certain physical conditions in the nucleus itself, but also occurs preferentially in certain specific environments. Indeed, the well-established steep evolution of the number density of luminous QSOs, taken together with the standard supermassive black hole model for such objects, indicates that less than 0.1% of the potentially active objects actually are active at the present epoch, implying that the necessary conditions for triggering QSO activity now occur only rarely. Detailed studies of the relations of QSOs to their environments have two principal justifications: (1) establishing firmer statistical bases for correlations between QSO activity and the properties of the environment and (2) seeking an understanding of the physical mechanisms underlying these correlations.

Observations of the immediate environments of QSOs at optical wavelengths have so far concentrated mainly upon the properties either of the galaxies in which QSOs are embedded or of the groups associated with these galaxies. Comparatively few studies have dealt with a third aspect of the environment: the extended ionized gas that surrounds a significant fraction of low-redshift QSOs. In this paper, we describe a general survey of a sample of luminous, low-redshift QSOs that we have carried out in order to estimate the frequency of occurrence of this extended emission, to search for correlations between its presence and other observed properties, and to discover suitable objects for further study. We plan in future papers to present more detailed observations and analyses of some of these objects.

The first QSOs found to have spatially resolved emission-line gas were 3CR 48 (Wampler *et al.* 1975) and 4C 37.43 (Stockton 1976). Both show rather easily detectable extended material on broad-band images, and it has since become clear that over certain regions near these and other objects, the emission from [O III] alone can dominate the total surface brightness over spectral bandpasses of 1000 Å or more.

Richstone and Oke (1977) discovered extended emission around 3CR 249.1 by means of a spectroscopic technique. More recently, we (Stockton and MacKenty 1983) obtained an image of this object through a narrow-band filter centered on the redshifted [O III] λ5007 line and found the ionized gas to be distributed principally in two extensive tail-like structures. We suggested that both the distribution of the ionized gas and the triggering of the QSO activity had resulted from a close interaction or merger of two galaxies. No velocities differing by more than 100 km s^{-1} from the systemic velocity were observed, indicating a low total mass for the system. In the same paper we also reported another luminous QSO with somewhat similar extended emission, Ton 202.

Boroson and Oke (1984) have observed the off-nuclear spectra of these and other luminous QSOs in an attempt to determine the properties of the extended luminous material. In addition to demonstrating convincingly the presence of A-type stars in the off-nuclear spectrum of 3CR 48, they observed extended line emission in many of the objects. Observations of additional objects and a summary of results from the enlarged sample have been given by Boroson, Persson, and Oke (1985).

[1] Visiting Astronomer, Canada-France-Hawaii Telescope, operated by the National Research Council of Canada, the Centre National de la Recherche Scientifique of France, and the University of Hawaii.

From a total sample of 12 high-luminosity QSOs and 12 low-luminosity objects, they found strong evidence linking the properties of the extended luminous component to the radio morphology and spectral index and to the character of the nuclear spectrum. The presence of strong extended emission lines was found to correlate with extended radio structure, a steep radio spectral index, broad and bumpy nuclear Balmer lines, strong nuclear narrow-line emission, and little or no nuclear Fe II emission. Objects for which the extended emission component is weak or absent tend to have compact, flat spectral index radio components, narrower and smoother nuclear Balmer lines, weak narrow-line emission, and prominent Fe II emission.

Our survey was begun without knowledge of Boroson and Oke's program but has fortuitously turned out to be complementary, since their survey was spectroscopic and we concentrated on imaging. We were originally motivated by a suspicion that the highly structured morphologies of the ionized gas distributions in 4C 37.43 and 3CR 249.1 must be transient phenomena and therefore might be causally connected in some way with the presence of the active nucleus (i.e., aside from the obvious possibility that the ionization depended on the nuclear UV continuum). The correlations found by Boroson and Oke (1984) raise other questions, such as the relationship of the extended ionized gas to the radio structure or to the classical narrow-line region. In order to make progress on these questions both imaging and spectroscopic observations will be necessary. Our survey consists primarily of narrow-band images centered on the redshifted [O III] λ5007 line for a sample of almost 50 high-luminosity QSOs, although we also have obtained nuclear spectra for all of the QSOs in our sample. In § II we outline the sample selection and discuss the observations; in § III we present descriptions of individual objects; in § IV we present results from an analysis of the sample as a whole; and in § V we discuss the implications these results have for our understanding of QSOs and the galaxies in which they are found. A brief summary is given in § VI.

II. OBSERVATIONS AND DATA REDUCTION

a) Sample Selection

The sample from which the observed objects were drawn comprised all QSOs known to us (as of mid–1983) with $z \leq 0.45$, $\delta > -25$, and $V < 5 \log z + 19.6$; in all there were 73 QSOs meeting these criteria. Three of these had redshifts placing the [O III] λ5007 line quite close to the Na D lines in the airglow and were therefore dropped from the sample. Our sample was further limited by the economics of acquiring the necessary narrow-band filters. Our strategy in purchasing filters was to first obtain those which, with small tilt adjustments, could accommodate several objects. We ended up with some two dozen filters, covering redshifted [O III] in 58 QSOs; the remaining 12 objects were sufficiently isolated in redshift that each would have required its own individual filter.

Because of constraints on observing time, only 47 of the QSOs for which suitable filters were available were observed, and observations varied considerably in quality and depth. The 11 objects not observed were not excluded randomly; several were judged unlikely to show significant extended emission on the basis of a correlation with the nuclear narrow-line emission found for the rest of the sample. We shall demonstrate in § IV that this bias is unlikely to affect our main conclusions.

b) Redshifts and Spectrophotometry

The spectroscopic observations had two objectives: determining accurate wavelengths for the [O III] λ5007 line for the sample so that the narrow-band filters could be centered accurately on the line, and obtaining information on the character of the spectrum—primarily absolute intensities of Hβ and [O III] $\lambda\lambda$4959, 5007.

We found early in our investigation that a substantial fraction ($\sim$15%) of the redshifts in the literature could not be trusted to place the [O III] λ5007 line within a 30 Å bandpass filter. There appear to be two reasons for such discrepancies: (1) published redshifts are generally an average of several lines, and substantial intrinsic redshift differences ranging up to $\sim$1000 km s^{-1} between broad and narrow lines are sometimes present; and (2) some of the redshift determinations, particularly those obtained with vidicon detectors, seem simply to have large errors. Because of this problem, we found it necessary to obtain new redshifts, based specifically on the [O III] lines, for our entire sample of QSOs. The observed [O III] λ5007 line redshifts come from a variety of sources: moderate dispersion photographic image-intensifier spectra, narrow-slit CCD spectra, and the wide-slit CCD spectra obtained for the spectrophotometric observations. Although the latter are not ideal for radial velocity measurements, we found in practice that errors due to miscentering the object in the slit could be kept below $\sim$3 Å.

Spectrophotometric observations under photometric conditions were obtained of the Hβ–[O III] $\lambda\lambda$4959, 5007 region for all objects in the sample. This spectroscopy was carried out with the University of Hawaii (UH) 2.2 m telescope's faint object spectrograph and the Galileo/Institute for Astronomy CCD system, using a Texas Instruments 500 × 500 CCD (Hlivak *et al.* 1982; Hlivak, Henry, and Pilcher 1984). After one-dimensional, sky-subtracted spectra had been extracted via standard reduction procedures, the wavelength linearization and photometric calibration were carried out by means of routines in the SPICA spectral reduction package at the Royal Observatory Edinburgh STARLINK node. The spectrophotometric standards were selected from the lists of Oke (1974) and Stone (1977), and the corrections for the atmospheric extinction (always quite small) were derived from fitting a three-component model (Hayes and Latham 1975) to mean Strömgren extinction coefficients for Mauna Kea.

The principal results of the spectroscopic program are given in columns (3)–(8) in Table 1. The redshifts given in column (3) apply specifically to the [O III] λ5007 line, unless that line was too weak to measure, in which case a redshift determined from Hβ is given in parentheses. Columns (4)–(7) give equivalent widths and luminosities for the nuclear Hβ and [O III] λ5007 emission, and column (8) gives the continuum luminosity at Hβ ($H_0 = 75$ km s^{-1} Mpc^{-1} and $q_0 = 0$ are assumed throughout this paper). The Hβ line strengths are likely to be systematically low, since we generally ignored any portion of the line profile underlying the [O III] $\lambda\lambda$4959, 5007 lines; however, the missing flux will seldom exceed 10% of the total. For a few objects, the [O III] line strengths are given as upper limits or not given at all: these are cases for which the λ5007 line is sufficiently weak that a significant fraction of any feature observed near the expected wavelength is likely to be Fe II λ5018.

TABLE 1

OBSERVED PROPERTIES OF QSO SAMPLE

(1)	(2)	(3)	(4)	(5)	(6)	(7)	(8)	(9)	(10)	(11)
			Hβ		[O III] λ5007		Continuum	Extended [O III]		
QSO	Name	$z_{[O\ III]}$	EW (Å)	log L (ergs s^{-1})	EW (Å)	log L (ergs s^{-1})	log L(λ) (ergs s^{-1} A^{-1})	log L_{TOT} (ergs s^{-1})	log L_{PK} (ergs s^{-1})	α_{400}^{2700} [a]
0003+158	4C15.01	0.4503	115	43.83	46	43.42	41.77	<42.40	<41.24	0.78
0017+257	4C25.01	0.2839	117	43.28	76	43.04	41.21	<41.84	<40.85	0.66
0052+251	PG	0.1542	74	43.01	32	42.62	41.14	$41.12^{+.22}_{-.44}$	40.66±.04	RQ
0100+020	PHL959	0.3936	96:	42.65:	28:	42.10:	40.67:	<42.50	...	RQ
0110+297	4C29.02	0.3622	198	42.52	223	42.54	40.23	<41.82	$41.38^{+.06}_{-.07}$	0.68
0130+033	PHL1027	0.3619	86	42.74	20	42.07	40.80	<41.10	<40.36	RQ
0134+329	3CR48	0.3689	70	43.04	84	43.12	41.19	$42.65^{+.06}_{-.07}$	41.92±.03	0.82
0137+060	PHL1092	(0.3958)	43:	43.66:	<11:	<42.08:	41.03	...	...	RQ
0137+010	NAB	0.3340	150	42.91	41	42.38	40.74	<41.39	<40.53	RQ
0151+045	PHL1226	0.4020:	64:	42.97:	19	42.43	41.15	<42.15	<40.98	RQ
0157+001	Mrk1014	0.1630	44	42.63	65	42.78	40.98	$41.71^{+.07}_{-.09}$	41.52±.03	RQ
0205+024	NAB	0.1553	62	42.87	37	42.60	41.08	$40.88^{+.07}_{-.09}$	40.84±.04	RQ
0752+258	OI287	0.4440:	160	43.39	221	43.48	41.20	<42.31	<41.45	1.07
0837-120	3C206	0.1980	21	42.42	30	42.49	41.09	<41.76	<40.78	0.78
0925-203	PKS	0.3469	79	43.15	39	42.80	41.26	<41.38	<41.05	0.27
1001+292	Ton28	(0.3291)	64	43.33	...	...	41.52	<42.20	<40.23	RQ
1004-217	PKS	(0.3304)	69	43.00	...	...	41.16	<41.31	<40.34	b
1004+130	4C13.41	0.2401	28	42.94	15	42.65	41.50	<41.29	<40.28	0.67
1011-282	PKS	0.2555	92	42.91	67	42.74	40.94	$42.32^{+.09}_{-.12}$	41.62±.04	0.85
1048-090	PKS	0.3450	76	43.17	48	42.97	41.29	<41.78	<40.82	0.78
1049-005	PG	0.3597	82	43.49	64	43.34	41.57	<42.17	<41.11	RQ
1049+616	4C61.20	0.4212	50	43.26	51	43.25	41.57	<42.39	<40.40	0.86
1058+110	4C10.30	0.4230	173:	42.98:	93:	42.76:	40.74	<41.46	<40.59	0.86
1100+772	3CR249.1	0.3120	48	43.30	56	43.33	41.61	42.72±.02	42.12±.01	(0.84)
1103-006	4C00.43	(0.428)	68	43.35	17:	42.76:	41.52	...	...	0.63
1121+422	PG	0.2244	111	42.99	9	41.88	40.95	...	...	RQ
1128+315	B2	0.2901	109	43.06	40	42.59	41.02	<41.53	40.36±.02	0.61
1146-037	PKS	0.3405	74	42.75	254	43.12	40.88	<41.95	<40.08	0.6:
1150+497	4C49.22	0.3334	118	42.88	43	42.43	40.80	<41.67	<40.30	(0.49)
1202+281	GQComae	0.1655	140	42.83	65	42.49	40.69	$40.09^{+.18}_{-.30}$	<40.23	RQ
1216+069	PG	0.3322	89	43.51	13	42.68	41.57	<42.00	...	RQ
1217+023	PKS	0.2405	79	43.02	43	42.71	41.12	<41.61	<40.41	0.47
1222+216	4C21.35	(0.434)	97	43.22	19:	42.51:	41.23	...	...	0.65
1223+252	4C25.40	0.2678	92	42.69	153	42.84	40.74	42.49±.02	41.72±.003	0.80
1226+023	3CR273	(0.1577)	95	43.99	<28	<43.43	42.01	<41.63	<40.40	0.19

TABLE 1— *Continued*

(1)	(2)	(3)	(4)	(5)	(6)	(7)	(8)	(9)	(10)	(11)
			Hβ		[O III] λ5007		Continuum	Extended [O III]		
QSO	Name	$z_{[O\ III]}$	EW (Å)	log L (ergs s^{-1})	EW (Å)	log L (ergs s^{-1})	log L(λ) (ergs s^{-1} A^{-1})	log L_{TOT} (ergs s^{-1})	log L_{PK} (ergs s^{-1})	α_{400}^{2700} [a]
1302-102	PKS	0.2790:	31	43.19	13	42.78	41.71	...	...	0.38
1307+085	PG	0.1541	73	42.84	39	42.53	40.97	<40.96	<40.38	RQ
1358+043	PG	0.4277	86	43.14	19:	42.50:	41.20	...	...	RQ
1402+261	PG	0.1648	90	42.89	...	...	40.94	...	...	RQ
1425+267	B2	0.3625	73	43.14	62	43.02	41.27	42.22±.04	41.89±.01	0.62
1444+407	PG	0.2672	78	43.15	...	...	41.26	...	...	RQ
1510-089	PKS	0.3595	97	43.14	8:	42.15:	41.15	...	...	0.10
1512+370	4C37.43	0.3708	85	43.28	75	43.18	41.35	42.87±.01	42.52±.004	0.80
1525+227	OR241	0.2537	37	42.54	27	42.41	40.98	<41.73	40.80±.09	0.75
1543+489	PG	(0.4010)	79	43.30	...	...	41.40	...	...	RQ
1545+210	3CR323.1	0.2645	55	43.03	47	42.92	41.29	42.10±.03	40.99±.02	0.71
1548+114	4C11.50	0.4357	127	42.66	174	42.81	40.56	42.52±.03	41.49±.03	0.72
1612+266	NAB	(0.3932)	94	42.75	...	...	40.78	...	...	RQ
1700+518	PG	(0.2919)	66	43.57	<5	<42.45	41.75	<41.54	<40.68	RQ
1704+608	3CR351	0.3714	9	42.44	34	43.01	41.47	<42.22	...	(0.74)
1745+163	MC3	0.3920	80	42.47	177	42.84	40.57	<41.83	41.29±.07	
2135-147	PKS	0.2005	59	42.96	77	43.05	41.19	41.74±.04	40.93±.07	0.79
2141+175	OX169	0.2103	60	42.93	9	42.10	41.15	$40.94^{+.07}_{-.08}$	40.57±.10	0.37
2201+315	4C31.63	0.2948	88	43.46	20	42.79	41.51	<41.95	<40.84	0.16
2233+134	PG	0.3262	68	42.78	23	42.28	40.94	<40.44	<39.30	RQ
2251+113	PKS	0.3254	120	43.33	38	42.84	41.26	42.37±.04	41.89±.01	0.73
2305+187	4C18.68	0.3128	139	42.18	343	42.66	40.03	<42.25	<41.22	0.73
2308+098	4C09.72	0.4330	60	43.10	22	42.64	41.33	<42.55	<41.48	0.90

[a] Radio spectral index α ($f_\nu \approx \nu^{-\alpha}$) between 400 and 2700 MHz. The spectral indices have been calculated from fluxes at 318 MHz (Condon and Jauncy 1974*a*, *b*), 365 MHz (Douglas *et al.* 1973; Ghigo and Owen 1973; Sharp and Bash 1975; Douglas *et al.* 1981), 408 MHz (Colla *et al.* 1970, 1972, 1973; Ekers 1969; Large *et al.* 1981), 468 MHz (Willis 1975), 2650 MHz (Ekers 1969; Wills 1975), and 2700 MHz (see Veron-Cetty and Veron 1984 for references). Values in parentheses are spectral indices between 178 and 2700 MHz, where the 178 MHz flux has been given by Gower, Scott, and Wills 1967.

[b] No low-frequency flux available; $\alpha_{2700}^{5000} = 0.0$ (Savage, Bolton, and Wright 1977).

c) *Images*

The [O III] images were obtained with both the UH 2.2 m telescope and the Canada-France-Hawaii 3.6 m telescope (CFHT), in all cases using the same CCD as was used for the spectroscopy. Generally (but not always), we would obtain the initial observation of an object with the smaller telescope, following up objects of particular interest with the CFHT. The filters for the [O III] imaging all had nominal widths (FWHM) of 30 Å; they could be tilted in 5 Å increments to shift the peak transmission to the blue by up to 25 Å

The raw CCD images were reduced by first subtracting the bias level and a scaled average of several dark frames, then dividing by a normalized flat-field exposure of a tungsten source diffusely reflected from the interior of the dome. This flat-field procedure worked quite well except when a strong airglow feature fell within the filter bandpass: in such cases, significant fringing is usually present.

We have used two methods to calibrate the [O III] images. For most of our images, we have calibration exposures of spectrophotometric standards obtained through the same filters; some, however, were obtained under nonphotometric conditions or do not have corresponding standard exposures for some other reason.

Those frames with calibration exposures were reduced in the following way. We define the effective width of a filter, w_e, to be the width of a filter with a square bandpass having the same integrated throughput and peak transmission as the actual

filter. Our filters all have similar profiles, and by integrating several transmission curves we have found that w_e can be closely approximated as $1.1w_h$, where w_h is the full width at half-maximum transmission. Using this approximation to the effective bandwidth, we derive a calibration from our standard-star observations allowing us to convert from counts s^{-1} to ergs cm^{-2} s^{-1} for this particular filter and instrumental configuration. When used to determine the total flux in an emission line, this procedure implicitly assumes that all of the flux in the line is concentrated at the filter peak. This approximation should be fairly good for the typical line widths and filter-centering accuracies involved.

Because we have spectrophotometric observations for every QSO imaged through our narrow-band filters, we can attempt a second calibration procedure: the flux in a spectrophotometric bandpass equal to w_e centered on the [O III] λ5007 line can be compared with the total count rate integrated over an area of the image corresponding to the effective entrance aperture for the spectrophotometry. This procedure allows the calibration of images obtained under nonphotometric conditions. For most of our images we can use both approaches and compare the results, as shown in Figure 1. Some individual objects show differences that are substantially larger than seems reasonable from random errors in the observations, and it is conceivable that these objects have actually varied in the typically several months between the spectroscopic and the imaging observations. However, there does not appear to be any substantial systematic effect; we therefore adopt the calibration based on the first approach where possible and the spectrophotometric calibration for the remaining cases.

Our goal at this stage is to quantify the extended [O III] emission in a manner that allows us to treat our sample as homogeneously as possible. In practice, this means that we must exclude from our consideration the region interior to a projected physical radius corresponding to the angular radius ($\sim 2''$) obscured by the scattered light from the QSO itself in the most distant members of the sample. We have therefore sought

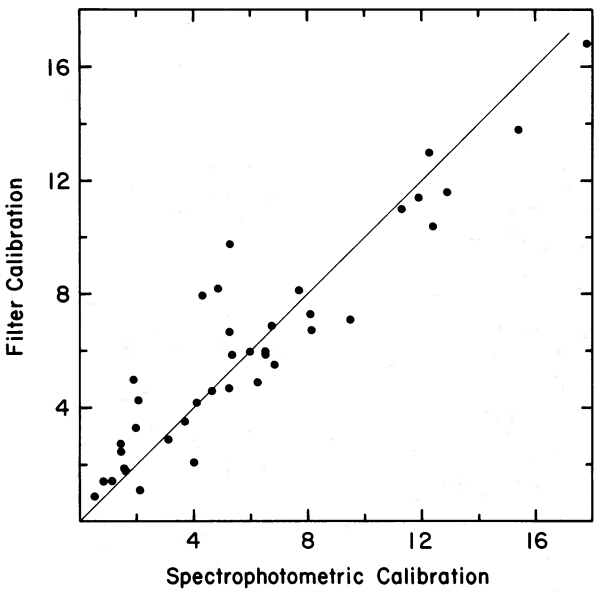

FIG. 1.—Comparison of filter and spectrophotometric calibrations for narrow-band [O III] images. The axes are labeled in units of 10^{-14} ergs s^{-1} cm^{-2}.

to determine the total luminosity in the [O III] λ5007 line in a projected annulus of inner radius 10 kpc ($H_0 = 75$ km s^{-1} Mpc^{-1}, $q_0 = 0$) and outer radius 40 kpc for each QSO for which we have narrow-band images. Limitations of the photometry software required us to reduce the size of the outer radius for a few of the lower redshift objects, but in no case did this limitation appear to have a significant effect on the results.

Certain corrections must be applied to this photometry in order to derive the [O III] luminosities. First, the wings of the stellar profile from the QSO nucleus contribute some light to the annulus measurement. This contribution was determined from identical measurements of stars on the frame; if no suitable stars were available, stars on adjacent exposures were used instead, at the expense of somewhat larger uncertainties. Second, extended continuum radiation will be present at some level. For most of the objects showing significant extended [O III] emission, we have obtained line-free continuum images as well. These images do not generally have good absolute calibrations, but a correction for the extended continuum luminosity can be derived by carrying out the same analysis as for the line images and scaling the corrected continuum flux from the annular region by a factor

$$\frac{q_e}{q_c}\frac{w_e}{E + w_e},$$

where q_e and q_c are, respectively, the intensities of the QSO itself in the emission-line and continuum images (the latter, of course, is in arbitrary units), E is the equivalent width of the [O III] λ5007 line in the QSO nucleus, and w_e is the effective filter width, as defined previously. This scale factor is simply the ratio of the *continuum* intensity at 5007 Å (in the emitted frame), given in ergs s^{-1}, to the continuum intensity at the wavelength sampled by the continuum filter, given in arbitrary units. It therefore uses the emission-line image as a calibration by correcting for the presence of the emission line, but it ignores any color difference between the continuum of the nucleus and that of the extended material. Since the separation between the continuum and the line passbands was typically only a few hundred angstroms, the error should not be large. Aside from the exceptional cases of 3CR 48 and Mrk 1014, the total luminosity of the extended continuum material in the annulus ranged from 3% to 9% of the nuclear continuum luminosity near 5000 Å. For those objects without continuum images, we have assumed the minimum value of 3% in order that our upper limits to the [O III] emission should be conservative ones. The corrected [O III] luminosities of the extended ionized gas are given in column (9) of Table 1. The 1 σ error estimates given are based on uncertainties in the photometry and in the corrections applied, and they are included in the upper limits given.

A somwhat unsatisfactory feature of the total annulus [O III] luminosity as a measure of the extended emission is that, although all of the detected examples are highly irregular and clumpy on scales of a few kiloparsecs, the upper limits are set by the smoothest possible distribution. Accordingly, we have considered a second measure as well: the maximum [O III] luminosity measured through an elliptical aperture with projected major and minor dimensions 20 kpc and 12 kpc, and unrestricted position and orientation, except that it lie wholly within the annular region defined above. The resulting luminosities and upper limits are given in column (10) of Table 1.

We have detected some sign of extended emission-line gas in 19 QSOs, out of the 47 with measurable emission-line images. For those objects with well-resolved [O III] λ5007 emission, the luminosities in the line within the annular aperture described above range over nearly three orders of magnitude, from 40.1 to 42.9 erg s^{-1}.

III. NOTES ON SPECIFIC OBJECTS

Figure 2 (Plates 4–8) shows [O III] images and, when available, line-free continuum images of all QSOs for which extended [O III] emission was detected. Insets, when present, generally show the central region around the QSO at lower contrast; in two cases (mentioned below), they instead show stars of similar brightness from the same frame for comparison, and in one (OX 169) the inset shows the continuum image. The horizontal bar on each print or pair of prints indicates 10″. In the comments on individual objects given below, the letter before the object designation is keyed to the illustration of the object in Figure 2. Following the coordinate designation of the object, a common name is given in parentheses. Occasionally, when the common name of an object does not reflect the fact that it is a radio-selected object, we have added the name of a major radio survey that contains it.

a) 0052+251 (PG)

The brightest region of extended line emission is seen ~3″.5 southeast of the QSO. Fainter filamentary structure is seen to the north and south of the QSO, covering a total projected range of over 50 kpc. The continuum material is also extended along the north-south direction but is much more smoothly distributed.

b) 0110+297 (4C 29.02)

No line-free continuum frame is available, but the extension to the east is not apparent on an *R* image obtained under only slightly poorer seeing conditions, and we believe that it is probably predominantly [O III] emission. The inset shows a star from the same frame for comparison.

c) 0134+329 (3CR 48)

This object, one of the first QSOs identified, was recognized to be slightly extended from the first deep images obtained (Matthews and Sandage 1963; Sandage and Miller 1966). It was also the first QSO shown to have a spatially resolved emission-line region (Wampler *et al.* 1975). Although in broad-band images the resolved structure extends both to the north and to the south, the character of the nebulosity differs in the two regions: ~4″ to the north, the emission-line spectrum dominates and the continuum is quite weak, while the same distance to the south the reverse is true (Wampler *et al.* 1975; Balick and Heckman 1983). Boroson and Oke (1982, 1984) have convincingly demonstrated that the continuum radiation is primarily due to A-type stars.

The north-south asymmetry in the properties of the extended component is clearly evident in our line and continuum images. The brightest emission-line region is a discrete object 3″ north of the nucleus, but there is diffuse ionized gas evident out to a radius of 4″ all along the north and west sides of the nucleus. The continuum radiation has its highest surface brightness to the south but its greatest extent to the northwest, where it takes on the appearance of a spiral-like feature reaching a projected distance of nearly 70 kpc from the nucleus. This feature has been noted by Gehren *et al.* (1984) and is barely visible on the reproduction of Sandage and Miller's (1966) image on the early experimental IIIa-J emulsion.

d) 0157+001 (Mrk 1014)

Continuum imaging and spectroscopic observations of the extended material have been discussed by MacKenty and Stockton (1984), who found stellar absorption lines from a mixture of early- and late-type stars in the bright spiral-like continuum feature. The continuum image displayed here is an improvement on our previous data, although the contrast level chosen does not show the broad "counter arm" as well. The line image shows several discrete emission regions that seem to be completely unrelated to the structure seen in the continuum. New spectroscopy of the bright spiral feature confirms the absorption-line spectrum reported earlier but also indicates that the equivalent width of [O III] λ5007 is quite small in this region: virtually all of the spiral feature seen in the line image is actually due to continuum radiation passed by the narrow-band filter. Unlike other galaxies present, the galaxy 20″ (50 kpc) to the west of Mrk 1014 appears enhanced and less centrally concentrated in the line image. These characteristics suggest that this galaxy is at the same redshift as Mrk 1014 and is also strong in [O III] λ5007; if so, its interstellar medium may have been ionized by radiation from the QSO.

e) 0205+024 (NAB)

There may be some very low surface brightness material visible on the line image to the north of the QSO, in the general direction of the small galaxy 8″.5 (21 kpc) away (this galaxy, like the one near Mrk 1014, appears to be enhanced on the emission-line image). However, the really striking feature in this pair of images is the unresolved object seen in the line image 12″ (29 kpc) to the east of the QSO, but absent from the continuum image; we estimate a lower limit of 400 Å to the equivalent width of the [O III] line. The reality of this object is confirmed by its appearance in images obtained on two successive months and by a recent spectroscopic detection of the [O III] $\lambda\lambda$4959, 5007 lines in it.

f) 1011−282 (PKS)

The strong fringing seen in this image results from the presence of the [O I] λ6300 airglow line within the bandpass. In spite of this problem, an arc of luminous material is clearly present, extending west and north from the south side of the QSO to a radial distance of 23″ (80 kpc). Although we do not have a continuum image for comparison, we do have spectroscopy confirming that this is emission-line radiation. A broad-band *R* image by Hutchings *et al.* (1984) shows a slight extension to the northwest of the QSO nucleus, which they suggest may be a faint galaxy. The arc of emission is projected onto the relaxed extended radio structure visible on the 20 cm VLA map of Gower and Hutchings (1984), but there is no detailed correlation between the two and no other evidence yet to suggest that they are closely related.

g) 1100+772 (3CR 249.1)

We have discussed these images in detail elsewhere (Stockton and MacKenty 1983) and briefly mention only our principal conclusions here. The structures of the extensions seen in the line image are strikingly reminiscent of tidal tails found associated with interacting or merging galaxies (note particularly that the straight tail on the northwestern side of the nucleus projects toward the northeastern end of the elon-

PLATE 4

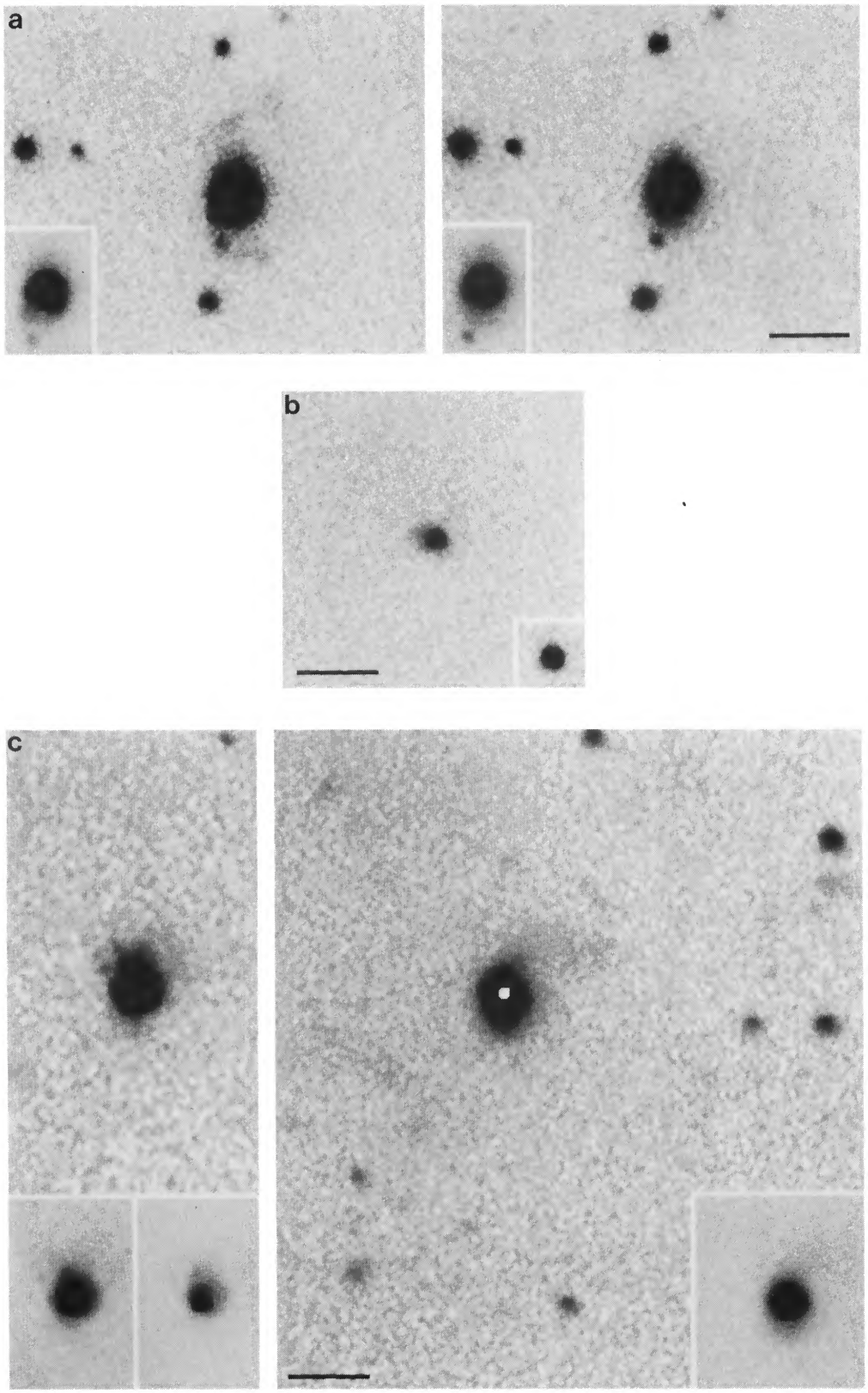

FIG. 2.—Images of selected QSOs. Where pairs of images are shown, the [O III] image is always at the left or top, the line-free continuum image at the right or bottom. Scale bars are 10″ long. Insets show lower contrast versions of the same image unless indicated otherwise. (*a*) 0052 + 251 (PG). (*b*) 0110 + 297 (4C 29.02). Inset shows a star for comparison. (*c*) 0134 + 329 (3CR 48). White dot on the continuum image indicates the position of the nucleus.

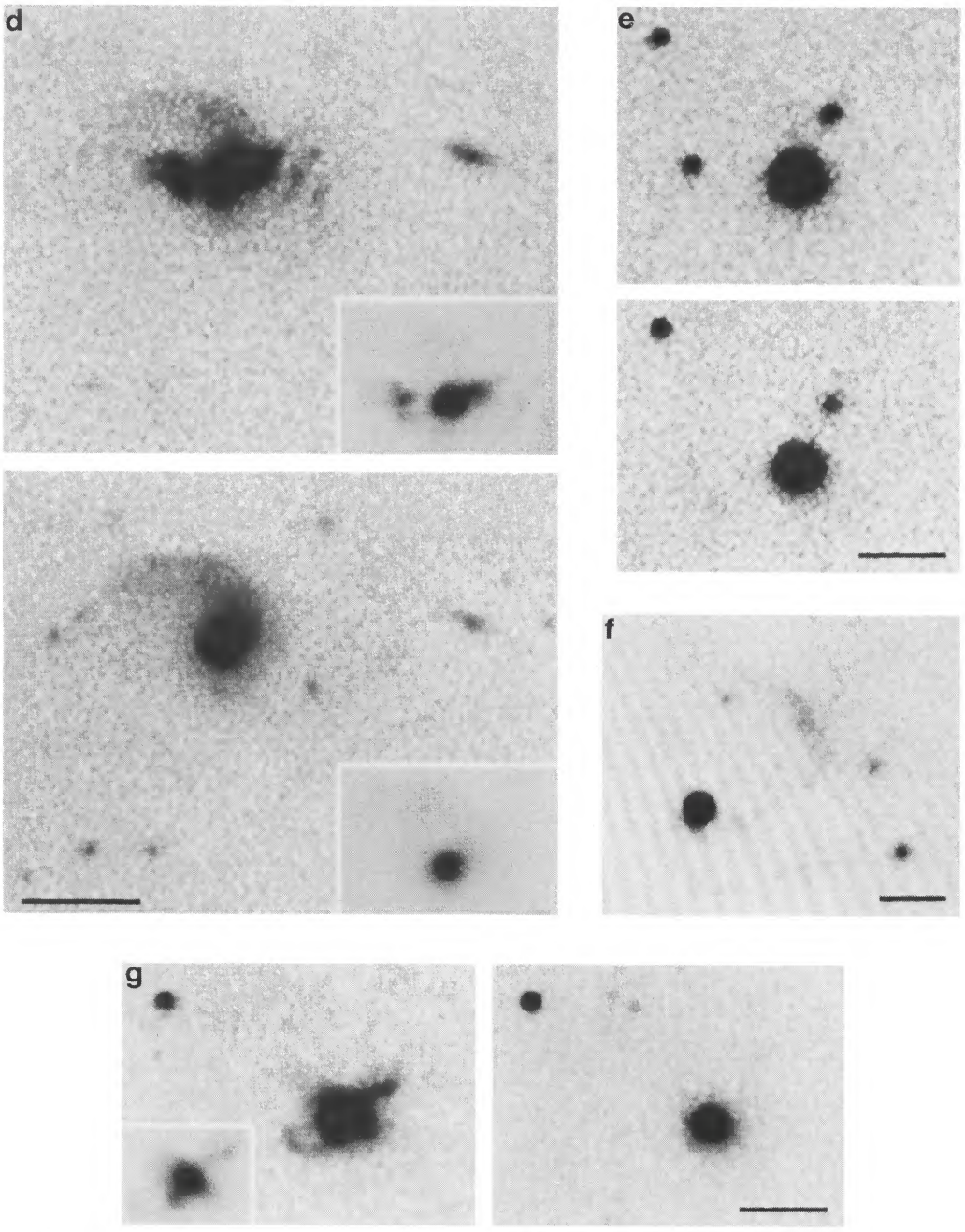

FIG. 2.—(*d*) 0157 + 001 (Mrk 1014). (*e*) 0205 + 024 (NAB). (*f*) 1011 − 282 (PKS). (*g*) 1100 + 772 (3CR 249.1).

PLATE 6

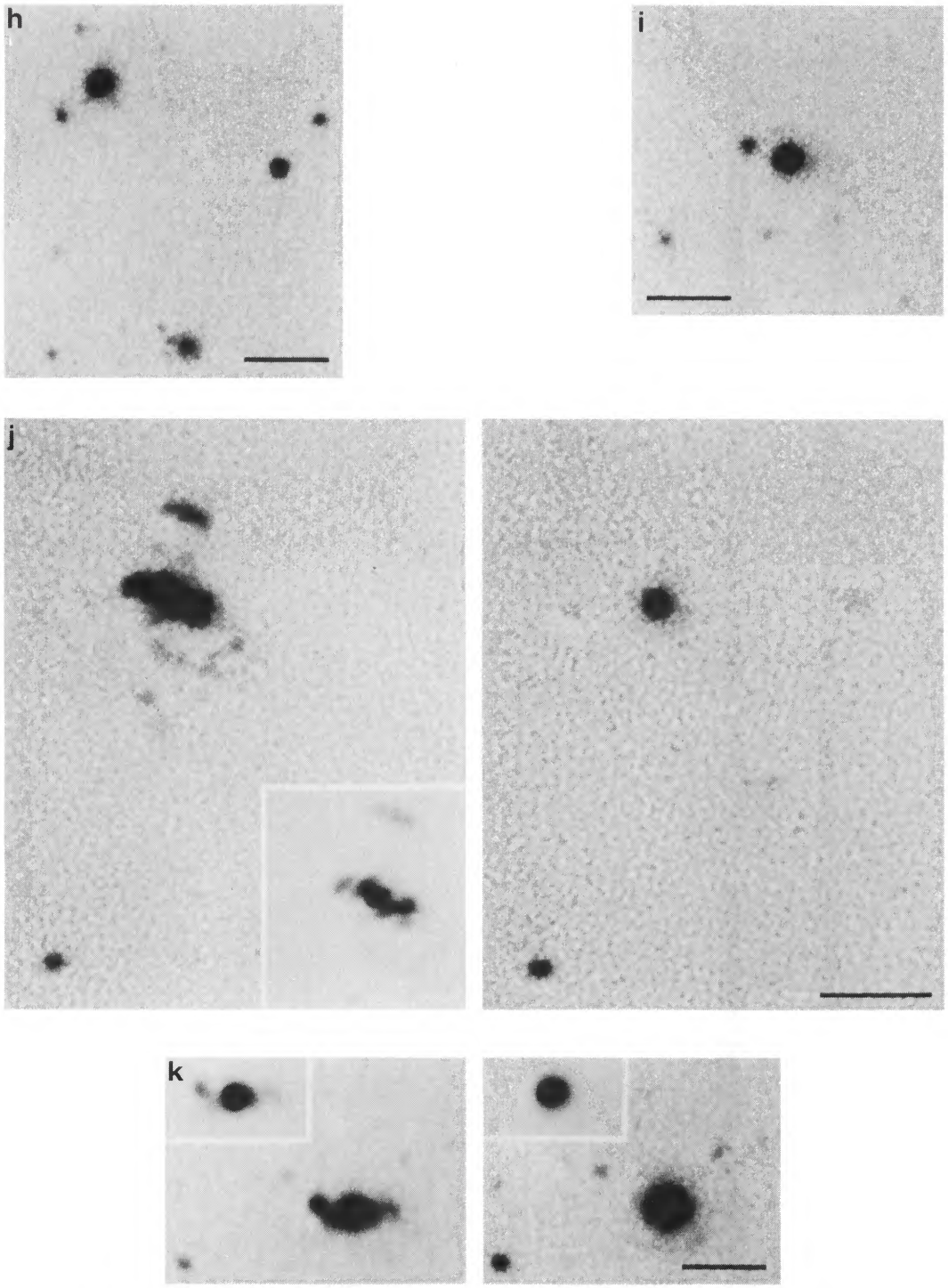

FIG. 2.—(*h*) 1128 + 315 (B2). (*i*) 1202 + 281 (GQ Comae). (*j*) 1223 + 252 (Ton 616, 4C 25.40). (*k*) 1425 + 267 (Ton 202, B2).

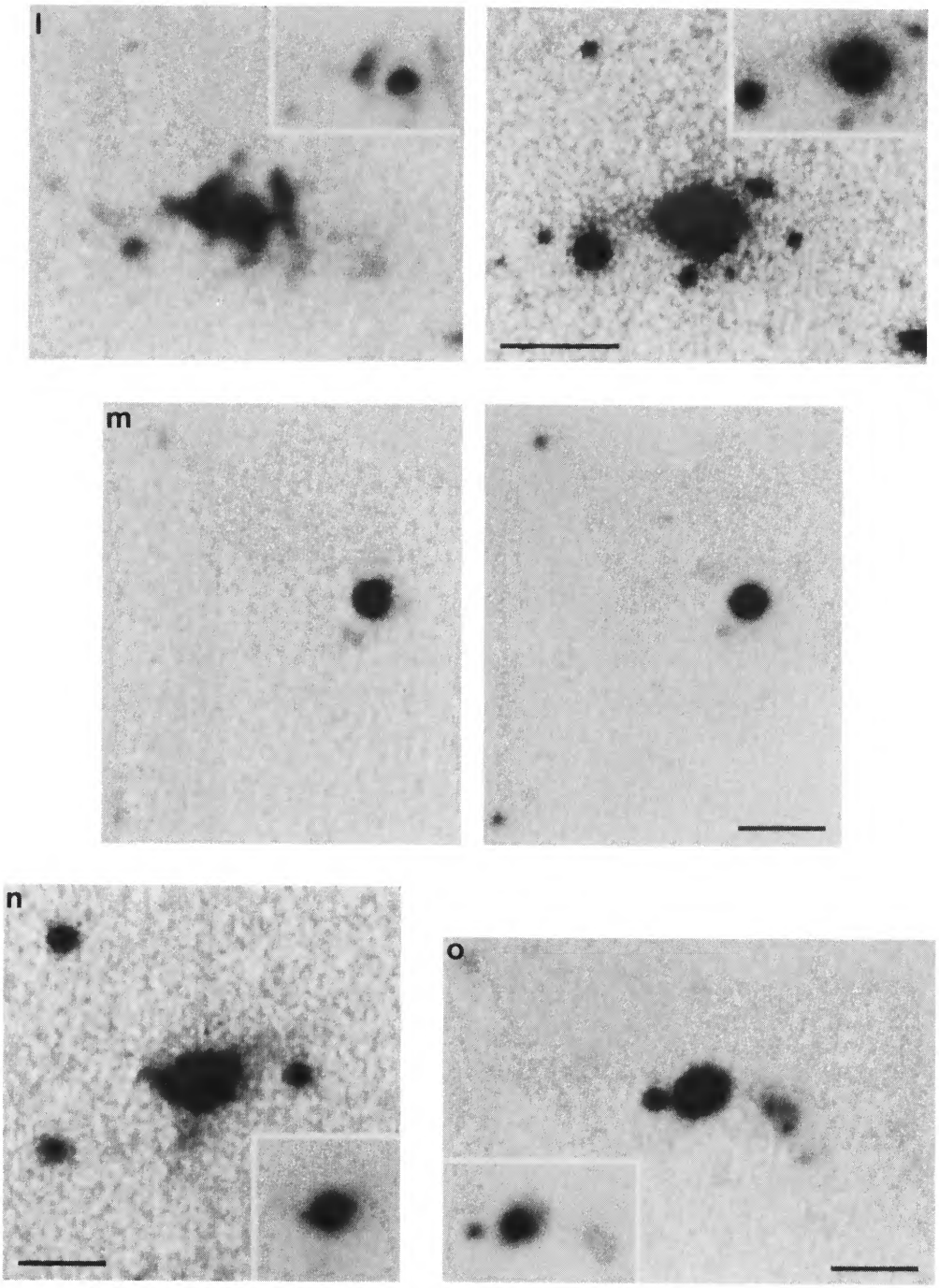

FIG. 2.—(*l*) 1512+370 (4C 37.43). Note that the insets in the two images are slightly displaced vertically relative to one another. (*m*) 1525+227 (LB 9743, B2). (*n*) 1545+210 (3CR 323.1). (*o*) 1548+114 (4C 11.50).

PLATE 8

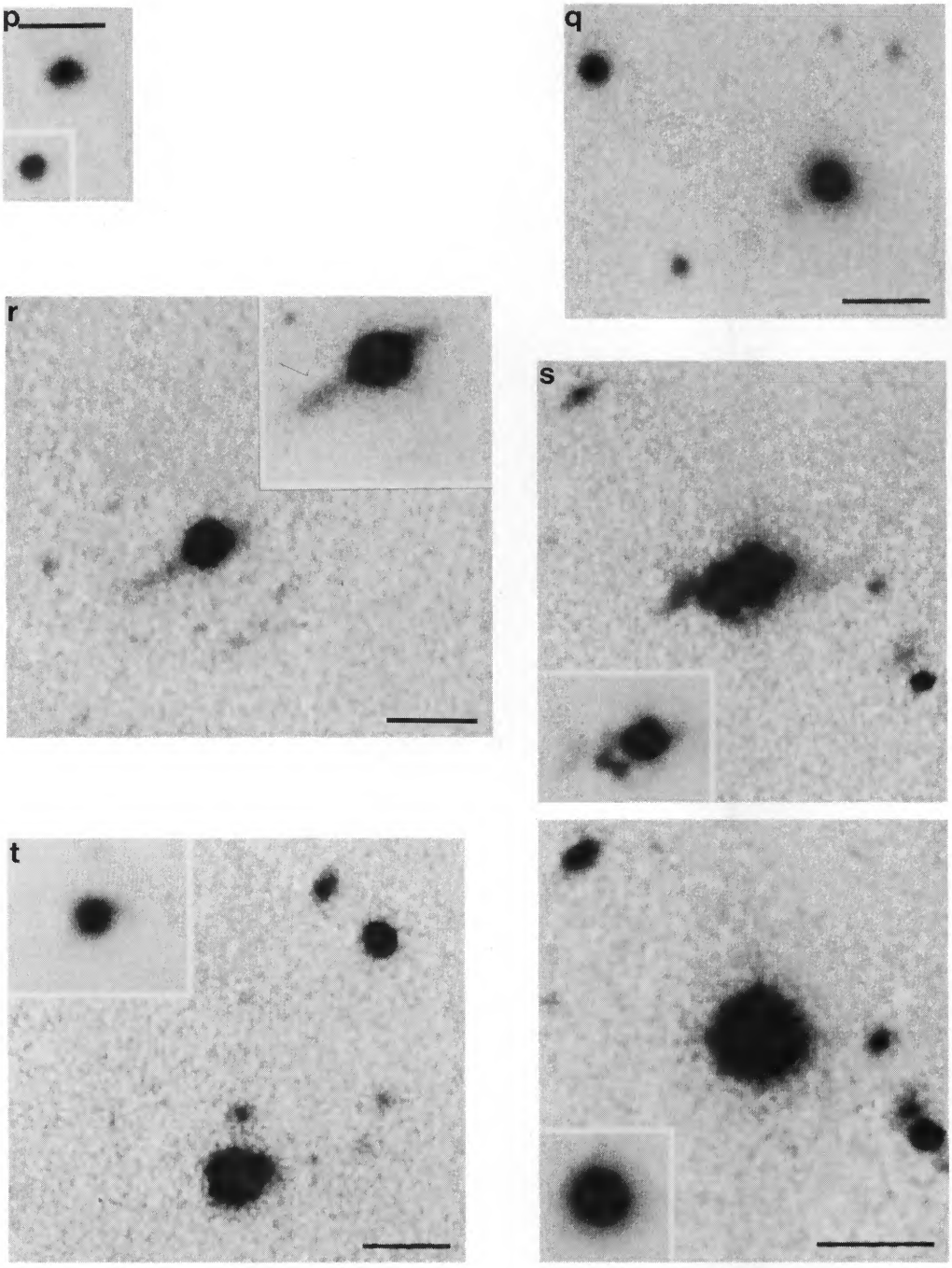

FIG. 2.—(*p*) 1745+163 (MC3). Inset shows a star for comparison. (*q*) 2135−147 (PKS). (*r*) 2141+175 (OX 169). Inset shows a line-free continuum image. (*s*) 2251+113 (PKS). (*t*) 2305+187 (4C 18.68).

gated envelope, rather than toward the nucleus). If these are indeed tidal features, two significant conclusions can be drawn: first, the presence of these narrow tails implies that both galaxies involved possessed cold gaseous disks prior to the interaction, suggesting that they may have been spirals. Second, because our fairly extensive spectroscopy uncovered no velocities in the gas exceeding 100 km s^{-1}, relative to the systemic velocity, the total mass involved is likely to be rather low. In both respects, the galaxy associated with 3CR 249.1 deviates from the giant ellipticals generally identified as the sites of activity leading to powerful extended radio sources.

h) 1128+315 (B2)

The extension to the southwest is a subtle feature compared with most of the others we discuss. We cannot even be completely certain that it is an emission-line feature rather than a continuum feature, although it does not appear to be present on a deep, broad-band, image-intensifier exposure obtained previously.

i) 1202+281 (GQ Comae)

The diffuse extension to the west of the QSO is almost certainly emission-line radiation because it is clearly absent on a deep prime-focus IIIa-F exposure obtained with the CFHT telescope in good seeing. Our spectroscopy confirms that the compact galaxy ~5″ to the east is at the same redshift as the QSO.

j) 1223+252 (Ton 616, 4C 25.40)

This object is one of the most complex and fascinating examples of an extended emission-line region found during our survey. The distribution of the bright emission regions in the immediate vicinity of the QSO nucleus appears to be inversion-symmetric (*see inset*), but, from another perspective, the two bright knots southwest of the nucleus could be interpreted as being part of the broken, off-center ring of much fainter material seen in the higher contrast principal illustration. At a projected distance of 7″.5 (28 kpc) to the north lies a completely detached, but quite luminous patch of ionized gas having no visible counterpart in the continuum image. At a somewhat greater distance to the south, past the ring, are two fainter emission regions.

k) 1425+267 (Ton 202, B2)

We have discussed this object previously (Stockton and MacKenty 1983) and give only a brief account here. Our suggestion that the two opposite extensions were tidal tails depend more on the velocity field than on the morphology of the ionized gas distribution. The strong asymmetry in the continuum image mentioned in our previous paper is not present in our new, deeper continuum image, shown here. Broad-band imaging data have also been presented by Hutchings *et al.* (1984) (the north direction indicated on their contour plot should apparently be west).

l) 1512+370 (4C 37.43)

Like that associated with 3CR 48, the extended ionized gas around 4C 37.43 was first detected on a broad-band image (Stockton 1976); but, while the narrow-band [O III] image of 3CR 48 shows little additional emission-line gas, that of 4C 37.43 reveals a complex distribution of fainter material extending over a region 31″ (140 kpc) across. The total luminosity in the extended [O III] emission is the largest of any object in our sample.

Although the distribution of the ionized gas is locally regular, in the sense that its organized into linear structures up to 30 kpc long, there seems to be little order or coherence among these units. It is striking how the two most luminous structures are aligned perpendicularly to the radial direction to the nucleus and are separated from it by gaps of over 10 kpc. The two faint emission regions farthest to the east appear to be aligned along an arc projecting toward the compact galaxy 10″ (45 kpc) east of the QSO, and associated with it (Stockton 1978).

Neither the distribution nor the velocity field (Stockton, in preparation) of the ionized gas offer any obvious insight into how an interaction between this galaxy and the QSO host galaxy could have produced the results we see. Nevertheless, the two almost certainly are interacting: as our continuum image shows, there appears to be a bridge, presumably of stars, connecting the two (Stockton 1986; Hickson and Hutchings 1987). A comparison of the line and continuum images shows that, while the extended luminous material is, in both cases, brightest to the east of the QSO, there is no detailed correlation between the two distributions.

m) 1525+227 (LB 9743, B2)

Gower and Hutchings (1984) have shown that the faint object 4″.9 (17 kpc) southeast of the QSO is coincident with the off-nuclear radio component of this D2 source. All our line image adds to the picture is the presence of [O III] emission ~1″.5 to the southwest of this object, and some diffuse emission to the west of the QSO itself.

n) 1545+210 (3CR 323.1)

While we have not obtained a line-free continuum image of this object, we do have deep, broad-band *R* image-intensifier and CCD images and can verify that the structure we see on our line image is indeed due to [O III] emission (however, the sharp spike to the east, seen in the low-contrast inset, is a column overflow from the saturated peak pixel of the QSO). The broad-band images show a compact object 2″.7 (9.7 kpc) northwest of the QSO; one of us has previously suggested (Stockton 1982) that this object is a compact galaxy that has interacted with the QSO host galaxy. Our present line image shows that the detection of [O III] emission in the spectrum of this object was fortuitous, since the emission is actually due to the general distribution of ionized gas surrounding the QSO. This development unfortunately leaves the nature of the compact object in some doubt, the redshift of the emission lines being the only firm basis for associating it with the QSO. A similar situation holds for PKS 2135−147 (see below). It still seems plausible that in both cases the compact objects are actually associated with the QSOs, since other similar associations have been confirmed (e.g., for Mrk 205, GQ Comae, and 4C 37.43).

o) 1548+114 (4C 11.50)

The fainter stellar object to the east is also a QSO, at a redshift of 1.901 (Wampler *et al.* 1973), and the tight group of three galaxies to the west is associated with the lower redshift QSO (Stockton 1978). The extended [O III] emission is less highly structured than in most other examples in our sample, the most noteworthy feature being a broad, diffuse fan toward the northwest. The luminosity gradient is much steeper on the

east side, toward the higher redshift QSO. Burbidge *et al.* (1977) have reported Mg II $\lambda\lambda$2796, 2803 absorption in the spectrum of the higher redshift QSO at a redshift of 0.4293, slightly lower than that of 4C 11.50 (0.4357). If there were emission-line gas near this absorption-line redshift, the [O III] λ5007 line would have been shifted out of our filter bandpass.

p) 1745+163 (MC3)

This object has a slight but definite extension, as can be seen by comparing the image with the field star from the same frame shown in the inset. Once again, we do not have a continuum frame for comparison, but Malkan (1984) describes this object as "not clearly resolved" by his broad-band imaging; if the extension we see were due to continuum emission, he would almost certainly have resolved it, so we feel secure in identifying the extension as line emission.

q) 2135−147 (PKS)

We have no line-free continuum image but do have a considerable amount of broad-band imaging data, and we can definitely state that virtually all of the extension seen in our line image is due to [O III] emission. This conclusion can be confirmed by examining the isophotal plot of an *R* image given by Hutchings *et al.* (1984); where the surface brightness of the galaxy 5".8 (17 kpc) to the southeast is clearly much higher than the extended material ~3" to the northeast of the QSO, whereas the reverse is true for our line image. Like 3CR 323.1, PKS 2135−147 has an apparent compact companion (Stockton 1982). It lies 2".0 southeast of the QSO; again like the companion to 3C 323.1, it is not enhanced in our line image, indicating that the emission lines seen in its spectrum are due to the general extended emission around the QSO rather than being intrinsic to the companion.

r) 2141+175 (OX 169)

The continuum image for this object is shown as an inset in the line image illustration. The jetlike feature toward the southeast and the corresponding short protruberance on the opposite side of the QSO are well-known (Stockton 1978; Hutchings *et al.* 1981, 1984; Gehren *et al.* 1984) but are shown somewhat better here than in previous work. Deep spectroscopic observations of this feature show it to be free of detectable emission lines, so its presence on our line image is due to continuum radiation in the bandpass. In fact, the only [O III] emission in this image comes from the region ranging from ~10" (30 kpc) south to the same distance southwest of the QSO, where several very faint emission knots are found, well separated from the QSO itself. This emission, though weak, is confirmed on two exposures obtained on different telescopes.

s) 2251+113 (PKS)

The most striking features of the line image are the two bright knots ~4" (16 kpc) southeast of the nucleus; these appear to be nearly coincident with the peak of the southeastern radio lobe on the 20 cm VLA map of Hintzen, Ulvestad, and Owen (1983). There are also several fainter diffuse patches, both to the east and the west of the QSO. The curving, tail-like feature extending at least 12" (50 kpc) to the west is present on two independent exposures. None of this fainter material is correlated with the radio structure.

t) 2305+187 (4C 18.68)

The host galaxy for this QSO is easily resolved in broad-band images (see, e.g., Hutchings *et al.* 1984; Shara, Moffat, and Albrecht 1985). We unfortunately do not have a line-free continuum image obtained with the same instrumental configuration for comparison, but we are not yet convinced that the extension seen on our line image or that of Shara *et al.* is anything more than continuum radiation. Qualitative comparisons are difficult, because the equivalent width of the [O III] λ5007 line in the QSO nucleus is over 300 Å, so the nucleus is greatly enhanced in the line image. Our line image appears to have a similar signal-to-noise ratio to that of Shara *et al.*, but we do not confirm the presence of the narrow feature found by them to extend northward from the east end of the envelope around 4C 18.68.

IV. CORRELATIONS BETWEEN THE EXTENDED EMISSION AND OTHER OBSERVED PROPERTIES

Early in our survey, we noticed that strong extended [O III] emission was present only for objects with at least moderately strong nuclear narrow-line emission (the converse, however, is not true). Figure 3 demonstrates this result for the whole sample: the distribution of nuclear [O III] luminosities for the objects with extended [O III] luminosities greater than 10^{42} ergs s^{-1} is clearly different from that for objects with extended [O III] luminosities less than this value. The objects plotted as dashed squares on the upper panel are those with *upper limits* to the extended [O III] luminosity greater than 10^{42} ergs s^{-1}. Since our upper limits for these objects are based on the unlikely circumstance of a uniform distribution of emission over our effective aperture and are only slightly above 10^{42} ergs s^{-1}, we suspect that tighter upper limits would place most of these objects on the lower panel. Note that the distribution of these 10 objects in $L_{N[O\ III]}$ is fairly uniform over the range

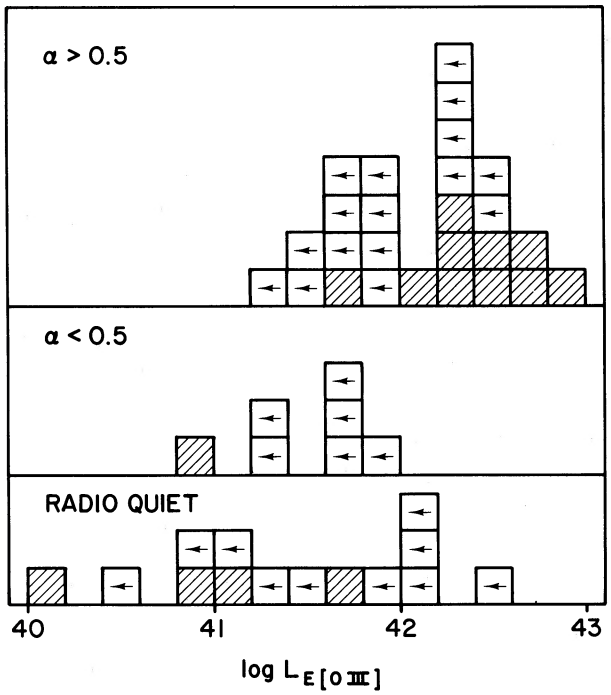

FIG. 3.—Histograms of nuclear [O III] λ5007 luminosity ($L_{N[O\ III]}$) for QSOs with extended [O III] λ5007 luminosities ($L_{E[O\ III]}$; see text for definition) above and below 10^{42} ergs s^{-1}.

shown on the plot, and that even a particularly perverse *anti-correlation* between extended and nuclear [O III] luminosities for this subset of objects could at most weaken but not destroy the observed correlation for the whole of the sample.

Also shown in Figure 3 is the distribution of nuclear [O III] luminosities of the objects for which we had no [O III] filters but which we did not observe. The choice of objects to omit clearly reflects our early perception of the correlation Figure 3 purports to demonstrate. However, we have observed a sufficient number of objects with weak nuclear [O III] emission to be reasonably confident that the five unobserved objects with $L_{N[O\,III]} < 10^{42}$ ergs s^{-1} are unlikely to hold any surprises.

A second correlation for our sample is shown in Figure 4, where histograms of extended [O III] luminosity are plotted for steep radio spectrum QSOs, flat radio spectrum QSOs, and radio-quiet QSOs. Nine of the steep radio spectrum sample have extended [O III] luminosities greater than 10^{42} ergs s^{-1}, whereas none of the flat-spectrum and radio-quiet objects do. The judgment of the eye is confirmed by nonparametric statistical tests incorporating the upper limits. If the radio-quiet and flat radio spectrum QSOs are combined, the Gehen, log-rank, and Peto-Prentice generalized Wilcoxon tests (Latta 1981; Schmitt 1985; Feigelson and Nelson 1985) all indicate that the distribution of the luminosities of extended [O III] emission for these QSOs differs from that for the steep radio spectrum QSOs at greater than the 99.9% confidence level.

These results only amplify and put on a more secure statistical footing correlations already noticed by Boroson and Oke (1984) and Boroson, Persson, and Oke (1985), who have emphasized that the separation of QSOs into two categories based on the presence or absence of strong extended emission also results in a separation according to radio properties and the character of the nuclear optical spectrum. The use of emission-line luminosities based on imaging data avoids the uncertainty associated with the incomplete spatial sampling of a slit spectrograph.

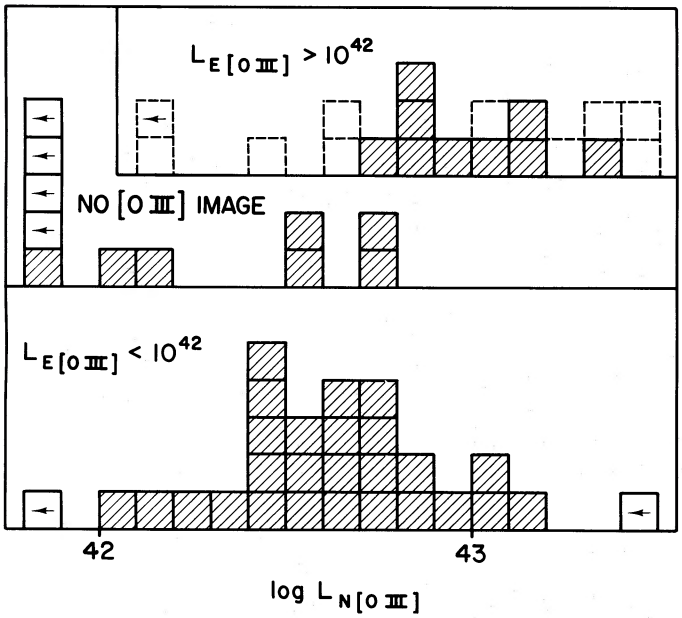

FIG. 4.—Histograms of the luminosity of extended [O III] λ5007 emission for steep radio spectrum, flat radio spectrum, and radio-quiet subsamples of QSOs.

Given the statistical correlation between the presence of extended ionized gas and steep-spectrum (i.e., usually extended) radio emission, it is of interest to summarize the evidence for cases of actual spatial correspondence between the two. All of the radio-loud QSOs in our sample that show strong extended optical emission have published VLA or Westerbork radio maps. Coincidences between optical and radio emission for three objects have been noted in § III. LB 9743 (1525+227) has a D2 radio morphology (Gower and Hutchings 1984) and weak extended optical emission. The principal off-nuclear concentration of emission-line gas is slightly displaced from the radio lobe but seems clearly to be related to it. PKS 1011−282 also has a predominantly D2 morphology, but with a peculiarly relaxed-looking radio structure between the central and off-nuclear components (Gower and Hutchings 1984). The extended optical emission lies projected on this region of diffuse radio emission, but it is not clear that the two are actually closely related. The strongest case for an association between strong extended emission-line gas and radio emission is PKS 2251+113, where the two brightest emission regions lie within 2″ on either side of the southeastern radio hot spot (Hintzen, Ulvestad, and Owen 1983). Even for this object, however, much of the extended emission is unrelated to the radio structure, and none is close to the position of the northwestern radio lobe.

These three are the only objects in our sample for which there is any substantial evidence for spatial correlations between optical and radio emission. We have also tried to test for the more general property of angular correlation by comparing the angular difference between the direction to the highest surface brightness emission-line region and the direction to the nearest radio hot spot. We were able to carry out this test for only eight objects, and the results from this small sample remain inconclusive: although for three objects the absolute value of this angle fell between 0° and 10°, for the remaining five objects it ranged from 28° to 65°.

V. DISCUSSION

Well over one-third of the steep radio spectrum QSOs in our sample show substantial, easily detected distributions of extended ionized gas. From the observed morphology of the gas, we infer that these structures, although sometimes highly organized, are transitory. Their high frequency of occurrence leads us to suspect that the presence of such extended gas is intimately connected in some way with the origin and development of the active nuclei in these objects. However, before we can speculate on the role such gas might play in the QSO phenomenon, we must try to answer a number of fundamental questions: What is the origin of the gas? How has it been ionized? What is its density and how is it confined? Does the distribution of the ionized gas we observe substantially reflect the actual gas distribution, or is our view of it controlled instead by shadowing or other effects that selectively ionize gas in certain regions only? Although we cannot yet give definitive answers to most of these questions, we have tentative indications for some of them.

a) Ionization Mechanism

Previous discussions of extended ionized gas around QSOs have assumed that the gas is photoionized by the UV continuum from the QSO itself (Wampler *et al.* 1975; Stockton 1976;

Richstone and Oke 1977; Stockton and MacKenty 1983; Boroson and Oke 1984; Boroson, Persson, and Oke 1985; Filippenko 1985). The principal basis for this assumption is the wide range of ionization states observed and the general similarity of the emission-line spectrum to that of classical narrow-line regions of active galaxies. Boroson and Oke (1984) have sufficient spectral coverage and signal-to-noise ratio to obtain fluxes for important diagnostic emission lines in the extended ionized gas of two objects, 3CR 249.1 and 4C 37.43. The ratios of [O II] λ3727 and Hβ to [O III] λ5007 are, respectively, 0.22 and 0.10 for both objects; these values place them firmly within the power-law photoionized domain (Baldwin, Phillips, and Terlevich 1981). Other line ratios as well are virtually identical in the two objects. The closeness of this agreement is no doubt fortuitous, but the fact that the ratios are similar can be taken as indicating an extremely well defined and consistent set of physical conditions. Detailed comparison shows that the line ratios cannot be reconciled with any of the wide range of shock ionization models calculated by Shull and McKee (1979) and by Raymond (1979).

Is the assumption that the extended gas has been photoionized by the nuclear UV continuum consistent with the observed line fluxes? Such analyses for extended ionized gas associated with two low-redshift radio galaxies have given mixed results. In one case (Fosbury *et al.* 1982), the UV luminosity of the nucleus seems just adequate to produce the observed line emission, provided that optically thick gas subtends most of the sky as seen from the nucleus. In the other (Danziger *et al.* 1984), one must invoke either local ionization sources or anisotropic radiation from the nucleus. For the low-luminosity QSO MR 2251 − 178 (Bergeron *et al.* 1983; Hansen, Norgaard-Nielsen, and Jorgensen 1984); however, only 5% of the UV continuum luminosity is needed to produce the observed extended line emission.

Table 2 gives, for each member of our QSO sample for which well-resolved extended emission has been detected, estimates of the fraction of the nuclear continuum radiation that must be intercepted by the gas (i.e., the "covering factor") in order to give the observed Hβ flux. These values have been calculated under the case B assumption, with the additional assumptions that the QSO continuum between Hβ and the Lyman limit is proportional to $\nu^{-0.4}$ (Soifer *et al.* 1983) and that the Hβ flux from the extended gas is 10% of the flux from [O III] λ5007. There are no glaring inconsistencies between these covering factors and the observed distributions of the ionized gas, and hence no evidence from this quarter that any ionizing source other than the nuclear continuum is necessary. Our continuum images give no hint that early-type stars might be associated with the emission regions; indeed, it is remarkable how completely divergent the distribution of any extended continuum component is from that of the emission-line gas.

TABLE 2

CALCULATED COVERING FACTORS OF EXTENDED IONIZED GAS

QSO	Covering Factor
0052+251.....	3.8×10^{-4}
0134+329.....	1.1×10^{-2}
0157+001.....	2.1×10^{-3}
0205+024.....	2.5×10^{-4}
1011−282.....	9.5×10^{-3}
1100+772.....	5.1×10^{-3}
1202+281.....	1.0×10^{-4}
1223+252.....	2.2×10^{-2}
1425+267.....	3.5×10^{-3}
1512+370.....	1.3×10^{-2}
1545+210.....	2.6×10^{-3}
1548+114.....	3.6×10^{-2}
2135−147.....	1.3×10^{-3}
2141+175.....	2.4×10^{-4}
2251+113.....	5.1×10^{-3}

We confirm, then, that the extended gas is almost certainly photoionized by the UV continuum from the QSO nucleus. Because the radiation density from the nuclear continuum source is typically a factor of $\sim$1000 lower at the position of the extended ionized component than it is in the nuclear narrow-line region, while the character of the spectra indicates that the ionization parameter is no more than a factor of 10 lower, the density of the extended gas must generally be less than $\sim$1% of the gas density of typical classical narrow-line–emitting clouds, which is $\sim 10^4$ cm^{-3}. *Mean* densities $\langle n \rangle$ over resolved regions (typically $\sim$3 kpc in extent) can be estimated from Hβ luminosities and the assumption that dimensions along the line of sight are similar to dimensions projected on the plane of the sky. For the highest surface brightness regions, $\langle n \rangle \approx 0.5$ cm^{-3}, providing a rough lower limit to the density of the emitting gas in these regions. The only direct estimate of the actual density of the emitting gas we have for any of these objects is a crude measurement of the ratio of the [O II] $\lambda\lambda$3726, 3729 doublet for the brightest region associated with 4C 37.43. The formal value for the electron density is 200 cm^{-3}, but the errors in the ratio are such that the low-density limit cannot be excluded. An accurate density measurement would be extremely valuable, since a knowledge of the density of the clouds and a discussion of the necessary confinement mechanisms could help decide the origin of the extended gas (see § V*c*).

b) The Distribution of the Extended Gas

We can summarize one aspect of our survey by noting two important properties of the extended ionized gas: first, it is generally highly structured, showing condensations and linear filaments, some of which have dimensions of tens of kiloparsecs; second, this structure appears to be almost completely independent of the distribution of any extended continuum material present. Whatever the origin of this extended gas, it is normally not simply the interstellar gas in the host galaxy ionized *in situ*.

In fact, the general anticorrelation between the extended ionized gas and the extended continuum material (presumably stars) is actually rather surprising: one might expect that at least sometimes these galaxies would contain normal interstellar gas that would be ionized by the central source. The most striking case in point is that of Mrk 1014 (Fig. 4*d*), where in spite of the presence of strong emission elsewhere, very little emission is found in the continuum spiral feature to the east (see § III*d*). Moderately early-type stars are present (MacKenty and Stockton 1984), so it seems unlikely that this region is completely devoid of gas. Instead, we suspect that it is shielded from the nuclear continuum radiation by an interior, coplanar distribution of dense gas: either gas associated with the inner disk, or possibly with the broad-line region clouds themselves.

The question of such shielding and the role it might play in the differences in the properties of the extended material between the steep radio spectrum, radio-loud QSOs on the one

hand and the flat-spectrum and radio-quet QSOs on the other has been discussed by Boroson, Persson, and Oke (1985). They propose, following Blandford (1984), that many of the observed correlations between this classification on the basis of radio properties and the characteristics of the optical spectra can be interpreted in terms of differing properties of the accretion disks surrounding the nuclear source. High flow rates produce thick accretion tori which soften the spectrum of the emergent radiation, resulting in smaller narrow-line regions and stronger Fe II lines in the broad-line region, and which also confine or quench the radio-emitting plasma. Below the critical accretion rate, the accretion disk remains thin, allowing both the UV flux and the radio plasma to escape.

A scheme of this sort is attractive, and selective shadowing of the photoionizing radiation seems to play a role in objects such as Mrk 1014. However, there are two reasons for believing that the extended gas is actually absent (at the relevant densities and temperatures) in some objects:

1. There are some steep radio spectrum QSOs with strong narrow-line emission that *do not* show any evidence of strong extended emission. (Note that, although many of the upper limits shown on Fig. 3 are in the same range as our detections, these upper limits are quite conservative because they are necessarily based on the assumption of the smoothest possible distribution of the emission, whereas the actual detections always show a highly structured distribution.) It is difficult to imagine that the UV continuum could suffer substantial extinction beyond the narrow-line region (except perhaps in a thin plane if a dense gaseous disk were present). We therefore tentatively conclude that, for those QSOs, the lack of detected extended emission is not due to lack of ionizing radiation, but to lack of gas.

2. For those QSOs that do show strong extended emission, the morphologies of the extended ionized gas features do not appear to be determined by shadowing of the ionizing radiation. On the contrary, they give every appearance of being density-limited, rather than radiation-limited, structures, and we therefore have reason to be confident that the distribution of ionized gas that we see is *primarily* determined by the actual density distribution of the gas. This general impression is susceptible to a test: if the distribution of ionized gas we see is controlled by variations in the absorption of ionizing radiation along various lines of sight from the nucleus, then the ionization parameter should generally be lower in regions of weaker emission, whereas the reverse would be true if the distribution is controlled by gas density variations. If the structure in most objects is density limited rather than radiation limited, it is entirely plausible that some objects simply do not have sufficient extended gas to produce a very luminous extended emission region.

These arguments do not exclude the possibility that many or most objects may still have a "zone of avoidance"—a plane in which any gas present is essentially shielded from the photoionizing continuum. We only caution that there must be real gas density variations as well and that the suggestion that the observed correlation of extended emission with extended radio structure can be explained entirely in terms of increased escape of UV photons remains speculative.

c) *Influence of the Local Environment*

There is evidence that radio-quiet QSOs (Yee and Green 1984) and flat-spectrum radio QSOs (Stockton 1978) occur less frequently in the more strongly clustered environments than do the steep-spectrum radio QSOs. If this result is confirmed, it could offer an alternative or supplementary explanation for the increased incidence of strong extended emission among the steep-spectrum QSOs. We consider two possibilities that might correlate with the local clustering amplitude:

1. The presence of the extended gas might have resulted from an interaction or merger (Stockton and MacKenty 1983). Such events will be more frequent in small groups than in the field.

2. The extended gas may be a cooled phase of a hot gas pervading the region, a group or cluster being necessary to provide the potential well to confine the hot gas.

For several objects showing strong extended emission, including 4C 37.43, 3CR 48, 3CR 323.1 Mkn 1014, and PKS 2135−147, there is independent evidence for recent interaction or merger: either close companion galaxies, or bridges or tails observed in continuum (presumably stellar) radiation, or both (Stockton 1982; Balick and Heckman 1983; MacKenty and Stockton 1984; Stockton 1986; Hickson and Hutchings 1987; this paper). It seems most economical to suppose that the presence of the extended ionized gas is connected with the interaction. The extended emission associated with GQ Comae is of lower luminosity than these other examples, but is directly opposite its close companion galaxy and is plausiby a countertidal feature. Examples of ionized gas reminiscent of tidal tails, such as that around 3CR 249.1 and PKS 2251+113, so far lack confirmation from observations of the stellar distribution but are nevertheless suggestive. In one similar case (Ton 202), the asymmetry in the velocities of the two tails favors an interaction (Stockton and MacKenty 1983).

We have emphasized the general lack of correlation between the distribution of extended continuum radiation and that of the ionized gas. If the gas has been ejected by tidal forces, either the gas and the stars originally had very different distributions or kinematics, or the present distribution of the gas has been largely controlled by hydrodynamic interaction with an intracluster medium. Such a medium would also help confine the gas, if indeed it actually is necessary that the gas be confined: the rather chaotic large-scale structure we observe in the emission-line gas does not encourage us to believe that the gas is in equilibrium. We typically resolve only features larger than ~ 3 kpc in these objects; with a sound speed of ~ 10 km s^{-1}, the dissipation time scale for a gas cloud 1 kpc across is $\sim 10^8$ yr. This time is of the same order as the interaction time scale.

If we consider instead the possibility that the emission-line gas has cooled from a hot surrounding medium, the structures we observe would be quasi-static features determined by the flow of the gas onto the QSO and confined by the pressure of the medium. Such cooling gas has been observed in clusters of galaxies, where cooling times for the hot X-ray-emitting gas are often found to be less than a Hubble time (see, e.g., Fabian *et al.* 1984). Cooling flows are inferred not only in rich, regular clusters, but also in some poorer clusters (Kriss, Cioffi, and Canizares 1983; Canizares, Stewart, and Fabian 1983) that come closer to approximating the typical environments of low-redshift, steep-radio-spectrum QSOs.

In some of the rich X-ray clusters, low-ionization optical emission is observed from the cooled gas (Hu, Cowie, and Wang 1985); this emission is believed to be due to shock excitation resulting from repressurization following thermal instability collapse. With a luminous QSO present, however, photoionization by the UV continuum from the QSO could

dominate the ionization of the gas and therefore control the characteristics of the observed emission-line spectrum.

How can we distinguish observationally between these two very different scenarios—interaction and cooling flow—for producing the emission-line gas? The most direct approach would be to search for hot X-ray–emitting gas in the QSO fields and estimate the cooling time for any hot gas found. This is a very difficult observation because the QSO itself is a point X-ray source that may be 100 times more luminous than the anticipated extended component, and it seems unlikely than any X-ray observatory prior to AXAF will have the resolution and aperture necessary to make much progress.

The density of the emitting gas could be a useful discriminant. We can estimate an upper limit to the density of 10^4 K gas in pressure equilibrium with an assumed hot intragroup medium as follows:

The cooling time for gas with number density $n\ (=n_p = n_e)$ and temperature T is

$$t_c = \frac{5kT}{n\Lambda(T)},$$

where $\Lambda(T)$ is the volume emissivity and is equal to $2 \times 10^{-27} T^{1/2}$ ergs cm^3 s^{-1} for thermal bremsstrahlung. This expression for Λ is a lower limit, since there may be additional cooling from line radiation. Thus we have an upper limit to the density:

$$n \leq 2.5 \times 10^{27} \frac{kT^{1/2}}{t_c}.$$

We take $t_c = 10^{10}$ yr as a conservative lower limit to the cooling time. An upper limit to the temperature of the gas comes from an estimate of typical velocity dispersions of galaxies in QSO groups. The line-of-sight velocity differences between QSOs and apparently associated galaxies given by Stockton (1978, 1980) have been recalculated using improved QSO redshifts and correction for observational errors to give a mean group line-of-sight velocity dispersion $\langle\sigma_G\rangle \approx 350$ km s^{-1} (this value should be considered an upper limit because of probable deviations of QSO emission-line redshifts from the center-of-mass redshifts as well as possible contamination from unbound galaxies). The corresponding temperature

$$T = \frac{m_p\langle\sigma_G\rangle^2}{k}$$

and $n \leq = 4 \times 10^{-3}$ cm^{-3}. Therefore the density of gas at 10^4 K in pressure equilibrium with this medium would be less than 6 cm^{-3}. Densities substantially above this value at large distances from the QSO would be difficult to explain in terms of a cooling flow model.

Another possibility[2] would be to look for chromospheric lines (such as [Fe X] λ6374 and [Fe XIV] λ5303) from gas at a temperature of $\sim 10^6$ K, which might be expected to form a sheath or cocoon between the cooler gas and the hotter X-ray gas. Also, if any substantial regions of space are shielded from the photoionizing continuum, one might find gas in these regions that retains the spectral signature of shock excitation.

It will be important to try these or any other tests that might serve to discriminate between alternative origins for the extended gas. At present, however, there is no independent evidence that cooling flows are occurring in the groups associated with the QSOs in our sample, and we suspect that the cooling flow interpretation has a better chance of being correct for the very different sort of extended emission found by Hintzen and Romanishin (1986) around the QSO 3CR 275.1 which appears to be in a rich cluster. We have cited evidence for interactions for a large fraction of the QSOs in our sample that show strong extended emission; we believe it likely that the ionized gas we see is debris from such interactions, but we cannot yet confirm this belief by physical modeling of the distribution and velocity fields of the gas.

d) A Connection with Intrinsic Absorption-Line Systems?

Whatever the provenance of the extended emission-line gas, its preferential association with steep-spectrum radio QSOs could offer an explanation for the apparent excess of QSOs with z(absorption) $\approx$ z(emission) among steep-spectrum radio QSOs found by Foltz *et al.* (1986)[3]. Any such identification of the absorbing clouds with the emission-line gas requires that the correlation between extended emission and radio spectral index found for $z < 0.45$ should remain valid for $z \approx 1.5$. While the velocity difference of up to 3000 km s^{-1} between the C IV λ1549 absorption and emission lines is large compared with the maximum 400 km s^{-1} difference found between the [O III] λ5007 emission from the extended gas and the nuclear narrow-line region, at least part of this discrepancy can be attributed to systematic deviations of the redshift of the C IV emission from that of the center-of-mass frame (Gaskell 1982).

VI. SUMMARY

We can summarize the major conclusions of our survey as follows:

1. While most previous mentions of extended ionized gas around QSOs have implicitly assumed the gas to be simply the interstellar medium of the QSO's host galaxy, we find that the ionized gas is not well correlated with the extended continuum material, as would be expected if it were normal interstellar gas.

2. In most of the objects we have observed, the distribution of the ionized gas is highly structured over scales of tens of kiloparsecs, but this structure is generally quite asymmetric and is clearly not that of gas in an equilibrium configuration.

3. Our results are consistent with the assumption that the extended gas has been ionized by the UV continuum from the QSO nucleus. There is suggestive evidence that some gas may be largely shielded from the nuclear source in at least one object (Mrk 1014), but most of the structure observed must be due to real density variations.

4. The correlations we find between the presence of strong extended emission and both the strength of the nuclear narrow-line emission and the radio spectral index generally confirm the results of Boroson and Oke (1984) and Boroson, Persson, and Oke (1985). However, some objects with both strong narrow-line emission and steep radio spectra seem not to have strong extended emission.

5. We believe that there is strong circumstantial evidence that the extended ionized gas is usually debris from interactions, but we cannot yet exclude other possibilities. The problematical cases on this interpretation are those where we see apparent tails of ionized gas, but no similar structure in the

[2] Suggested to us by L. Cowie.

[3] This possibility was pointed out to us by J. Bergeron.

extended continuum; deeper continuum images will be required in order to resolve this question. The alternative suggestion of Fabian, Nulsen, and Canizares (1986) that the extended ionized gas is cooled intracluster gas may apply in some cases, such as 3CR 275.1 (Hintzen and Romanishin 1986), but there is no evidence so far that the small groups with which the QSOs in our sample are typically associated contain gas at the necessary densities.

Whether or not we are correct in our specific interpretation of the origin of the extended gas will ultimately be of far less importance than the fact that these impressive structures must bear *some* close connection with the nuclear activity of the QSO. We are confident that more detailed investigations of certain of these objects will prove to be important in identifying at least one of the mechanisms by which strong nuclear activity is initiated and sustained.

We have discussed aspects of this survey with many people over the past 2 years. We wish to thank Jacqueline Bergeron and Len Cowie for reading early versions of this manuscript and offering helpful suggestions, and the latter, particularly, for a number of discussions. A. S. thanks the Astronomer Royal for Scotland, Professor Malcolm Longair, for arranging for his stay at the Royal Observatory Edinburgh, where most of the detailed data reduction and some of the writing of this paper was carried out. He is also grateful for support from NSF grant AST 83-17457, as is J. W. M. for support from the Honolulu chapter of the ARCS Foundation.

REFERENCES

Baldwin, J. A., Phillips, M. M., and Terlevich, R. J. 1981, *Pub. A.S.P.*, **93**, 5.
Balick, B., and Heckman, T. M. 1983, *Ap. J. (Letters)*, **265**, L1.
Bergeron, J., Boksenberg, A., Dennefeld, M., and Tarenghi, M. 1983, *M.N.R.A.S.*, **202**, 125.
Blandford, R. D. 1984, *Ann. NY Acad. Sci.*, **442**, 303.
Boroson, T. A., and Oke, J. B. 1982, *Nature*, **296**, 397.
———. 1984, *Ap. J.*, **281**, 535.
Boroson, T. A., Persson, S. E., and Oke, J. B. 1985, *Ap. J.*, **293**, 120.
Burbidge, E. M., Smith, H. E., Weymann, R. J., and Williams, R. E. 1977, *Ap. J.*, **218**, 1.
Canizares, C. R., Stewart, G. C., and Fabian, A. C. 1983, *Ap. J.*, **272**, 449.
Colla, G., *et al.* 1970, *Astr. Ap. Suppl.*, **1**, 281.
———. 1972, *Astr. Ap. Suppl.*, **7**, 1.
———. 1973, *Astr. Ap. Suppl.*, **11**, 291.
Condon, J. J., and Jauncey, D. L. 1974*a*, *A.J.*, **79**, 437.
———. 1974*b*, *A.J.*, **79**, 1220.
Danziger, I. J., Fosbury, R. A. E., Goss, W. M., Bland, J., and Boksenberg, A. 1984, *M.N.R.A.S.*, **208**, 598.
Douglas, J. N., Bash, F. N., Ghigo, F. D., Moseley, G. F., and Torrence, G. W. 1973, *A.J.*, **78**, 1.
Douglas, J. N., Bash, F. N., Torrence, G. W., and Wolfe, C. 1981, *Univ. Texas Pub. Astr.* No. 17, p.1.
Ekers, J. A., ed. 1969, *Australian J. Phys. Ap. Suppl.*, **7**, 1.
Fabian, A. C., Arnaud, K. A., Nulsen, P. E. J., and Mushotzky, R. F. 1986, *Ap. J.*, **305**, 9.
Fabian, A. C., Nulsen, P. E. J., Canizares, C. R. 1984, *Nature*, **310**, 733.
Feigelson, E. D., and Nelson, P. I. 1985, *Ap. J.*, **293**, 192.
Filippenko, A. V. 1985, *A.J.*, **90**, 1172.
Foltz, C. B., Weymann, R. J.. Peterson, B. M., Sun, L., Malkan, M. A., and Chaffee, F. H. 1986, *Ap. J.*, **307**, 504.
Fosbury, R. A. E., *et al.* 1982, *M.N.R.A.S.*, **201**, 991.
Gaskell, C. M. 1982, *Ap. J.*, **263**, 79.
Gehren, T., Fried, J., Wehinger, P. A., and Wyckoff, S. 1984, *Ap. J.*, **278**, 11.
Ghigo, F. D., and Owen, F. N. 1973, *A.J.*, **78**, 848.
Gower, A., and Hutchings, J. B. 1984, *A.J.*, **89**, 1658.
Gower, J. F. R., Scott, P. F., and Wills, D. 1967, *Mem. R.A.S.*, **71**, 49.
Hansen, L., Norgaard-Nielsen, H. U., and Jorgensen, H. E. 1984, *Astr. Ap.*, **136**, L11.
Hayes, D. S., and Latham, D. 1975, *Ap. J.*, **197**, 593.
Hickson, P., and Hutchings, J. B. 1987, *Ap. J.*, **312**, in press.
Hintzen, P., and Romanishin, W. 1986, preprint.
Hintzen, P., Ulvestad, J., and Owen, F. 1983, *A.J.*, **88**, 709.
Hlivak, R. J., Henry, J. P., and Pilcher, C. B. 1984, *Proc. SPIE.*, **445**, 122.
Hlivak, R. J., Pilcher, C. B., Howell, R. A., Colucci, A. J., and Henry, J. P. 1982, *Proc. SPIE.*, **331**, 96.
Hu, E. M., Cowie, L. L., and Wang, Z. 1985, *Ap. J. Suppl.*, **59**, 447.
Hutchings, J. B., Crampton, D., Campbell, B., Duncan, D., and Glendenning, B. 1984, *Ap. J. Suppl.*, **55**, 319.
Hutchings, J. B., Crampton, D., Campbell, B., and Pritchet, C. 1981, *Ap. J.*, **247**, 743.
Kriss, G. A., Cioffi, D. F., and Canizares, C. R. 1983, *Ap. J.*, **272**, 439.
Large, M. I., Mills, B. Y., Little, A. G., Crawford, D. F., and Sutton, J. M. 1981, *M.N.R.A.S.*, **194**, 693.
Latta, R. B. 1981, *J. Am. Statistical Ass.*, **76**, 701.
MacKenty, J. W., and Stockton, A. 1984, *Ap. J.*, **283**, 64.
Malkan, M. A. 1984, *Ap. J.*, **287**, 555.
Matthews, T. A., and Sandage, A. 1963, *Ap. J.*, **138**, 30.
Oke, J. B. 1974, *Ap. J. Suppl.*, **27**, 21.
Raymond, J. C. 1979, *Ap. J. Suppl.*, **39**, 1.
Richstone, D. O., and Oke, J. B. 1977, *Ap. J.*, **213**, 8.
Sandage, A. R., and Miller, W. C. 1966. *Ap. J.*, **144**, 1238.
Savage, A., Bolton, J. G., and Wright, A. E. 1977, *Australian J. Phys. Ap. Suppl.*, **44**, 1.
Schmitt, J. H. M. M. 1985, *Ap. J.*, **293**, 178.
Shara, M. M., Moffat, A. F. J., and Albrecht, R. 1985, *Ap. J.*, **296**, 399.
Sharp, J. R., and Bash, F. N. 1975, *A.J.*, **80**, 335.
Shull, J. M., and McKee, C. F. 1979, *Ap. J.*, **227**, 131.
Soifer, B. T., Neugebauer, G., Oke, J. B., Matthews, K., and Lacy, J. H. 1983, *Ap. J.*, **265**, 18.
Stockton, A. 1976, *Ap. J. (Letters)*, **205**, L113.
———. 1978, *Ap. J.*, **223**, 747.
———. 1980, in *IAU Symposium 92, Objects of High Redshift*,, ed. G. O. Abell and P. J. E. Peebles (Dordrecht: Reidel), p. 89.
———. 1982, *Ap. J.*, **257**, 33.
———. 1986, *Ap. Space Sci.*, **118**, 487.
Stockton, A., and MacKenty, J. W. 1983, *Nature*, **305**, 678.
Stone, R. P. S., 1977, *Ap. J.*, **218**, 767.
Vernon-Cetty, M.-P., and Vernon, P. 1984, *ESO Sci. Rept.*, No. 1.
Wampler, E. J., Baldwin, J. A., Burke, W. L., and Robinson, L. B. 1973, *Nature*, **246**, 204.
Wampler, E. J., Robinson, L. B., Burbidge, E. M., and Baldwin, J. A., 1975, *Ap. J. (Letters)*, **198**, L49.
Wills, B. J. 1975, *Australian J. Phys. Ap. Suppl.*, **38**, 1.
Yee, H. K. C., and Green, R. F. 1984, *Ap. J.*, **280**, 79.

JOHN W. MACKENTY: Space Telescope Science Institute, Homewood Campus, Baltimore, MD 21218

ALAN STOCKTON: Institute for Astronomy, 2680 Woodlawn Drive, Honolulu, HI 96822